On the semiclassical initial value calculation of thermal rate coefficients for the N + N 2 reaction

N. Faginas Lago, A. Laganá, R. Gargano, and P. R. P. Barreto

Citation: The Journal of Chemical Physics **125**, 114311 (2006); doi: 10.1063/1.2345363
View online: http://dx.doi.org/10.1063/1.2345363
View Table of Contents: http://scitation.aip.org/content/aip/journal/jcp/125/11?ver=pdfcov
Published by the AIP Publishing

On the semiclassical initial value calculation of thermal rate coefficients for the N+N_2 reaction

N. Faginas Lago[a] and A. Laganá[b]
Department of Chemistry, University of Perugia, Via Elce di Sotto, 8-06123 Perugia, Italy

R. Gargano[c]
Instituto de Física, Universidade de Brasilia, Caixa-Postal 04455, 70919970 Brasilia, Distrito Federal, Brazil

P. R. P. Barreto[d]
Laboratório Associado de Plasma, Instituto Nacional de Pesquisas Espaciais, CP 515, So Jos dos Campos 12201-970, Sao Paulo, Brazil

(Received 12 June 2006; accepted 4 August 2006; published online 20 September 2006)

In this paper we compare semiclassical initial value representation, conventional transition state theory with Wigner and Eckart tunneling correction, quantum reduced dimensionality, and quasiclassical thermal rate coefficients for N+N_2 exchange reaction. © *2006 American Institute of Physics*. [DOI: 10.1063/1.2345363]

I. INTRODUCTION

Recently there has been renewed interest in the study of the

$$N(^4S_u) + N_2(^1\Sigma_g^+, \nu) \rightarrow N(^4S_u) + N_2(^1\Sigma_g^+, \nu') \quad (1)$$

reaction. The key motivation for this is the need for modeling the reentering of spacecrafts landing on the solar planets whose atmosphere contains a large amount of nitrogen.[1–7] This implies the need for calculating extended matrices of accurate detailed rate coefficient values of the various processes of reaction (1). In spite of that, for this reaction only little experimental information[8–10] on the dependence of the rate coefficients from the temperature is available. Moreover, also theoretical information is quite scarce. In particular, the only potential energy surface (PES) available from the literature is the London-Eyring-Polanyi-Sato (LEPS)PES having a collinear transition state 36 kcal/mol higher in energy than the asymptotes.[11] More recently, a PES formulated as an exponential multiplied by an expansion in terms of Legendre polynomials has been fitted to 3326 *ab initio* points calculated using a coupled cluster singles and doubles correction method with perturbation correction of triples.[12] On this PES [Wang-Stallcop-Huo-Dateo-Schwenke-Partridge (WSHD-SP)]three dimensional zero total angular momentum calculations of the reactive probabilities have been performed. The unavailability of a copy of the WSHDSP PES has motivated us to still use the old LEPS PES to improve our understanding of the system and to compare the suitability of the semiclassical (SC) method in calculating the rate coefficient of reaction (1). After all, most of the work to be used for comparison has been already performed[11,13] using the LEPS PES (including some recent zero total angular momentum quantum calculations of reactive and nonreactive probabilities[1]).

In the present paper, we compare and discuss the thermal rate coefficient values obtained using the SC initial value representation (IVR) approach with those calculated using the conventional transition state theory (TST) (with Wigner and Eckart tunneling corrections), the quantum reactive infinite order sudden (RIOS), and the full dimensional quasiclassical trajectory (QCT) methods on the LEPS PES. The aim of the paper is also that of providing a unified computational scheme to assemble the workflow manager of the so-called grid enabled molecular simulator (GEMS) being built within the EGEE European project.[14]

The paper is articulated as follows: in Sec. II we briefly outline the theoretical methods used and in Sec. III we discuss and compare the results obtained.

II. THEORETICAL ESTIMATES OF THERMAL RATE COEFFICIENTS

Thermal rate coefficients for bimolecular atom diatom reactions at a given temperature T can be expressed as

$$k(T) = \frac{1}{Q_{\text{vib}}(T)Q_{\text{rot}}(T)} \sum_{\nu} \sum_{j} \sum_{\nu'} \sum_{j'} w_j k_{\nu j,\nu' j'}, \quad (2)$$

where w_j is the rotational state multiplicity including the nuclear spin symmetry and $k_{\nu j,\nu' j'}$ is the state to state rate coefficient defined as

$$k_{\nu j,\nu' j'}(T) = (Q_{\text{trans}})^{-1} \int E_{\text{tr}} \sigma_{\nu j,\nu' j'}(E_{\text{tr}}) e^{-E_{\text{tr}}/k_B T} dE_{\text{tr}}. \quad (3)$$

In Eq. (3) $\sigma_{\nu j,\nu' j'}$ is the state to state cross section (unprimed quantities for reactants, primed ones for products), k_B is the Boltzmann constant, Q_{trans}, Q_{vib}, and Q_{rot} are the translational, vibrational and rotational partition functions, respectively, and E_{tr} is the relative translational energy. As usual, the partition functions are formulated as

[a]Also at Department of Physical Chemistry, University of Basque Country, Vitoria, Spain
[b]Electronic mail: noelia@dyn.unipg.it
[c]Electronic mail gargano@fis.unb.br
[d]Electronic mail: patricia@plasma.inpe.br

$$Q_{\text{trans}} = \left(\frac{\mu k_B T}{2\pi\hbar^2}\right)^{3/2}, \tag{4}$$

$$Q_{\text{vib}}(T) = \sum_{\nu} \exp(-\varepsilon_\nu / k_B(T)), \tag{5}$$

$$Q_{\text{rot}}(T) = \sum_{j} w_j \exp(-\varepsilon_j / k_B T), \tag{6}$$

where $\hbar$ is the Planck constant, ε_ν and ε_j are the energies of the vibrational (ν) and rotational (j) states, respectively. For reaction (1) w_j is equal to $6(2j+1)$ for even rotational numbers and $3(2j+1)$ for odd rotational numbers, and μ is the reduced mass of the system in the reactant atom diatom arrangement ($\mu = 2m_N/3$ with $m_N = 14.0067$). The calculation of the state to state cross section $\sigma_{\nu j,\nu' j'}$ is, therefore, the key step of any dynamical *a priori* evaluation of the state to state rate coefficient. The state to state cross section can be either computed individually (at various levels of accuracy) or incorporated into a more averaged evaluation of reactive fluxes at some intermediate dividing surface when only the thermalized rate coefficient is required.

A. The full three dimensional dynamical quantum and quasiclassical calculations of the cross section

The most accurate approach to the calculation of $\sigma_{\nu j,\nu' j'}$ is the integration of either the time independent or the time dependent Schrödinger equation. A crucial difficulty of this method of evaluating $\sigma_{\nu j,\nu' j'}$ is the large quantity of coupled differential equations which needs to be integrated before convergence with total angular momentum is reached when a full dimensional approach is followed. At present, most of the quantum calculations for heavy atom diatom systems are still carried out only for null total angular momentum quantum number (J) and then, in a more or less empirical way, $J=0$ results are extended to higher J values (see Refs. 1 and 12 for $N+N_2$). Full three dimensional calculations of the state to state cross section are, instead, straightforwardly performed using QCT means. In our case the quasiclassical state to state cross section was calculated by integrating a five dimensional integral over the initial unobservable conditions using a Monte Carlo technique leading to the following expression:[14]

$$\sigma_{\nu j,\nu' j'} = \frac{\pi b_{\max}^2}{M} \sum_{i=1}^{\dot{M}} f_{\nu j,\nu' j'}(\xi_1, \xi_2, \xi_3, \xi_4, \xi_5). \tag{7}$$

In Eq. (7) the ξ_i's are pseudorandom numbers, M is the number of events (trajectories) considered for the Monte Carlo integration, $b_{\max}$ is the maximum value of the impact parameter leading to reactive encounters, and $f_{\nu j,\nu' j'}(\xi_1, \xi_2, \xi_3, \xi_4, \xi_5)$ is a Boolean function whose value is 1 only when, after integrating the related trajectory starting from the νj quantum state of the reactants, the final outcome can be assigned to the $\nu' j'$ quantum state of the products and zero otherwise.

B. The reduced dimensionality dynamical quantum calculation of the cross section

Due to the already mentioned difficulty of carrying out, even with presently available computer power, a fully converged three dimensional quantum calculation of the state to state cross section of the $N+N_2$ system, quantum calculations can be performed at the already mentioned RIOS level.[15,16] In the RIOS scheme, the detailed cross section $\sigma_{\nu j,\nu' j'}$ is approximated in terms of the ground rotational state cross section $\sigma_{\nu j=0,\nu'}$ values using the relationships $\sigma_{\nu j,\nu' j'}(E_{\text{tr}}) = \sigma_{\nu j=0,\nu'}(E_{\text{tr}} - \varepsilon_\nu - \varepsilon_j)$ and $j' = l$ (with l being the orbiting quantum number of the rigid atom diatom system). Then, the ground rotational state cross section is formulated as

$$\sigma_{\nu j=0,\nu'}(E_{\text{tr}}) = \frac{\pi}{k_\nu^2} \sum_{l} (2l+1) \times \int_{-1}^{1} |S_{\nu l,\nu'}(\Theta; E_{\text{tr}})|^2 d\cos\Theta. \tag{8}$$

where $k_\nu^2 = 2\mu(E - \varepsilon_\nu)$, Θ is the angle formed by the reactant mass scaled Jacobi coordinates R (atom-diatom distance) and r (diatom internuclear distance), E is the total energy, and $S_{\nu l,\nu'}$ is the fixed angle RIOS vibrational state to state element of the scattering matrix at a given value of l. The scattering matrix is evaluated by integrating the coupled differential equations obtained from the RIOS formulation of the Schrödinger equation,[16]

$$\left[-\frac{\hbar^2}{2\mu}\left(\frac{1}{R}\frac{\partial^2}{\partial R^2}R + \frac{1}{r}\frac{\partial^2}{\partial r^2}r - \frac{A_l}{R^2} - \frac{B_j}{r^2}\right) + V(R,r;\Theta)\right]\Xi(R,r;\Theta) = E\Xi(R,r;\Theta), \tag{9}$$

where $A_l = \hbar^2 l(l+1)$, $B_j = \hbar^2 j(j+1)$, and $\Xi(R,r;\Theta)$ is the fixed Θ RIOS wavefunction.

C. Direct semiclassical calculation of the rate coefficients

The semiclassical rate coefficient that retains the full dimensionality character of the classical approach, while regaining the quantumlike nature of the scattering process, can be formulated as [17–20]

$$k(T) = \frac{1}{Q_{\text{trans}}(T) Q_{\text{vib}}(T) Q_{\text{rot}}(T)} \int_0^\infty dt C_{ff}(t), \tag{10}$$

with $C_{ff}(t) = R_{ff}(t) * C_{ff}(0)$. The "static" factor $C_{ff}(0)$ can be calculated exactly using imaginary-time path integral techniques, while the "dynamical" factor $R_{ff}(t)$, also called flux correlation function, can be evaluated approximately through the combined use of the SC-IVR and path integral scheme.

The static factor $C_{ff}(0)$ is expressed as (see Ref. 20)

$$C_{ff}(0) = 2\left(\frac{4k_B T}{\hbar}\right)^2 \{\text{tr}[h(\hat{s}) e^{-3\hat{H}/4k_B T} h(\hat{s}) e^{\hat{H}/4k_B T}] - \text{tr}[h(\hat{s}) e^{-\hat{H}/2k_B T} h(\hat{s}) e^{-\hat{H}/2k_B T}]\}, \tag{11}$$

that can be simplified by interposing the identity relation

$h(\hat{s})+[1-h(\hat{s})]=1$ between all the $e^{-4\hat{H}/k_BT}$ factors and canceling divergent contributions.

The flux correlation function is expressed as

$$R_{ff}(t)=\frac{C_{ff}(t)}{C_{ff}(0)}\sim\left\langle\frac{\langle\mathbf{q}_t'\mathbf{p}_t'|\hat{F}(1/2k_BT)|\mathbf{q}_t\mathbf{p}_t\rangle}{\langle\mathbf{q}_0'\mathbf{p}_0'|\hat{F}(1/2k_BT)|\mathbf{q}_0\mathbf{p}_0\rangle}\times C_t(\mathbf{q}_0\mathbf{p}_0)C_t^*(\mathbf{q}_0'\mathbf{p}_0')\times e^{i[S_t(\mathbf{q}_0\mathbf{p}_0)-S_t(\mathbf{q}_0'\mathbf{p}_0')]/\hbar}\right\rangle_W, \tag{12}$$

with $\langle\cdots\rangle_W$ being a Monte Carlo average over W. In Eq. (12) $(\mathbf{q}_0\mathbf{p}_0;\mathbf{q}_0'\mathbf{p}_0')$ are the initial and final coordinates and momenta for a single classical trajectory running from time 0 to time t. In the same equation S_t is the classical action, C_t is the square root of a determinant that involves the various monodromy matrices, and $\hat{F}(1/2k_BT)$ is the Boltzmannized flux operator chosen to have an intermediate form between the traditional "half split"[21] and the "Kubo"[22] one,

$$\hat{F}(1/k_BT)=\frac{2k_BT}{\hbar}[e^{-\hat{H}/4k_BT}h(\hat{s})e^{-3\hat{H}/4k_BT}-e^{-3\hat{H}/4k_BT}h(\hat{s})e^{-\hat{H}/4k_BT}]. \tag{13}$$

The actual evaluation of $R_{ff}(t)$ was further simplified (see Ref. 23) to avoid the computation of the monodromy matrix.

D. Transition state theory calculation of the rate coefficient

For sake of completeness we have also considered the traditional TST approach in which the atom diatom rate coefficient for N+N_2 can be written as[24,25]

$$k_{\mathrm{TST}}=\frac{k_BT}{\hbar}\frac{Q_{N_3^{\ddagger}}(T)}{Q(T)}\exp\left(-\frac{V_a^G}{\mathcal{R}T}\right), \tag{14}$$

where $\mathcal{R}$ is the universal gas constant, $Q_{N_3^{\ddagger}}$ and $Q(T)$ are the partition functions of the transition state (taken at the saddle point and labeled as $N_3^{\ddagger}$) and of the reactants, respectively, defined as a product of the related Q_{trans}, Q_{rot} and Q_{vib}. In the same equation V_α^G is the sum of $V^{\ddagger}$, the classical potential energy at the transition state saddle, and the E[zero point energy (ZEP)] is energy difference of transition state and reactants, as it is calculated in this case.

The corresponding TST rate coefficient expression corrected for quantum transmission reads

$$k_{\mathrm{TST}}^{W/E}(T)=\kappa^{W/E}(T)k_{\mathrm{TST}}(T), \tag{15}$$

where $\kappa^{W/E}(T)$ is either the Wigner $(\kappa^W(T))$ or the Eckart $(\kappa^E(T))$ transmission coefficient.

The Wigner correction for tunneling, based on the assumption that near the transition state the potential has a parabolic shape,[24,26] reads as

$$\kappa^W(T)=1+\frac{1}{24}\left|\frac{\hbar\omega^{\ddagger}}{k_BT}\right|^2, \tag{16}$$

with $\omega^{\ddagger}$ being the imaginary frequency at the saddle point.

TABLE I. Equilibrium internuclear distance, frequency, and dissociation energy of reactant/product N_5.

re_{N_2} [Å]	1.009
ωN_2	2358.87
D_e [kcal mol^{-1}]	228.41

The Eckart tunneling correction is estimated instead by solving the Schrödinger equation for the Eckart potential barrier.[27] Then, $\kappa^E(T)$ is obtained from the ratio between the quantum mechanical and the classical rate constant calculated by integrating the associated transmission probabilities over the entire energy range,

$$\kappa^E(T)=\frac{\exp(-V_a^G/k_BT)}{k_BT}\int_0^{\infty}\exp(-E_{\mathrm{tr}}/k_BT)\Gamma(E_{\mathrm{tr}})dE_{\mathrm{tr}}. \tag{17}$$

In Eq. (17) $\Gamma(E_{\mathrm{tr}})$ is the transmission probability that for the Eckart model potential has a simple trigonometric formulation (see Refs. 27–29).

III. CALCULATIONS AND RESULTS

A. The potential energy surface and its features

As already mentioned the PES used for our calculations is the LEPS of Ref. 13. Table I shows the equilibrium internuclear distance (r_{eN_2}), the frequency (ω_{N_2}), and the dissociation energy (D_e) of both reactant and product asymptotes.

Figure 1 shows an ensemble of fixed Θ minimum energy path (MEP) graphs for the N+N_2 reactive process using a pseudo-three-dimensional representation. The fixed Θ MEPs were constructed by cutting the R,r plane by straight lines centered on a high-in-energy turning point located on the ridge separating reactant and product channels. The evolution from reactants to products is obtained by rotating the cutting line by an angle ϕ (at $\phi=0°$ the line is parallel to r, while at $\phi=90°$ the line is parallel to R).

The plot clearly shows that the lowest saddle is placed at $\Theta=180°$, while the height of the saddle increases in going towards $\Theta=90°$ (perpendicular approach). A more quantita-

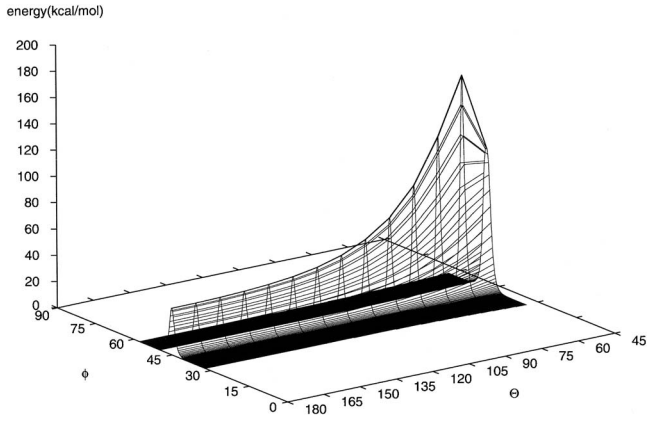

FIG. 1. Pseudo-three-dimensional plot of an ensemble of fixed Θ minimum energy paths calculated at different values of ϕ for the N+N_2 exchange reaction (see the text for the definition of Θ and ϕ). The energy zero was set at the entrance channel asymptote.

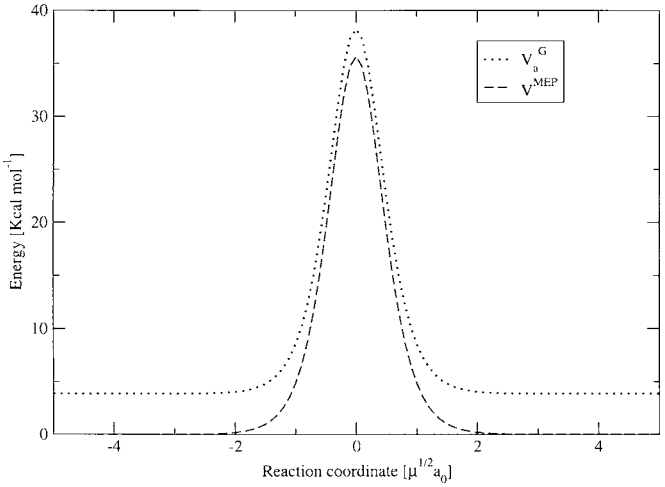

FIG. 2. MEP (dashed line) and related V_a^G (dotted line) plotted as a function of the reaction coordinate.

tive picture of the collinear MEP and of the evolution along it of the zero point energy (approximated as the ground vibrationally adiabatic harmonic energy) is given in Fig. 2, where both quantities are plotted as a function of the reaction coordinate defined as in Ref. 30–32 as a function of the MEP. The figure clearly shows that the difference between the V_a^G and the MEP curve smoothly decreases in going from the asymptotic towards the strong interaction region.

B. Computational details

QCT estimates of the thermal rate coefficient were calculated by running batches of 10^6 trajectories. The initial conditions of the trajectories were randomly selected to lead to vibrational and rotational distributions mimicking the Boltzmann one for the temperature considered. The temperature values considered were $T=500$, 1000, 2000, and 4000 K.

RIOS estimates of the thermal rate coefficient were calculated by computing the detailed cross section for a range of energy extending up to 200 kcal/mol in steps of about 2 kcal/mol. The fixed Θ **S** matrix elements were calculated by dividing the interval of the propagation coordinate in 200 sectors and expanding the wave function using sector basis sets of 20 functions. The values of Θ considered for the angular integration of Eq. (9) are regularly spaced in cos Θ using a step of 0.0625.

TST estimates of the thermal rate coefficient were calculated using the computational procedure developed by Barreto and co-workers.[30–32] The related code determines the MEP and calculates related harmonic frequencies. Table II shows the coordinates, frequencies (ω_1 is the symmetric stretch, ω_2 is the asymmetric stretch, and ω_3 is the bending), and height of the TST saddle configuration.[33–35]

SC-IVR estimates of the rate coefficient were obtained using a slightly more complex computational procedure articulated into the following steps: In the first step, 10^6 trajectories are integrated for a temperature interval ranging from $T=200$ K to $T=4000$ K in steps of 200 K to build the flux correlation function. The initial conditions of real-time trajectories $(\mathbf{q}_0,\mathbf{p}_0)$ and $(\mathbf{q}_0',\mathbf{p}_0')$ are sampled using the standard Metropolis method and the following weight function:

TABLE II. Internuclear distances, frequencies and energy of TST saddle configuration for the $N+N_2$ reaction.

$\tau N_a N_b$ (Å)	1.279 9209
$\tau N_b N_c$ (Å)	1.232 93965
$\theta N_a N_b N_c$	180°
ω_1 (cm^{-1})	242.644
ω_2 (cm^{-1})	1323.150
ω_3 (cm^{-1})	940.644i
$V^{\ddagger}$ (kcal mol^{-1})	35.67

$$W(\mathbf{q}_0\mathbf{p}_0;\mathbf{q}_0'\mathbf{p}_0') \sim |\langle \mathbf{q}_0\mathbf{p}_0|\hat{F}(1/2k_BT)|\mathbf{q}_0'\mathbf{p}_0'\rangle|. \quad (18)$$

In the second step the "static" factor $C_{ff}(0)$ of Eq. (11) is computed by converting the problem into that of determining a partition function. This is achieved by first introducing a "variable" dividing surface separating the reactant from the product region whose location and shape are adjusted to minimize the number of recrossing trajectories. The characteristics of the partition function in the asymptotic region at the chosen reference temperature are determined using the discrete variable representation[36] (DVR) method.

In the third step the dynamic factor $R_{ff}(t)$ is evaluated by determining the characteristics of the partition function in the interaction region in terms of its ratio with that of the asymptotic region at the reference temperature using the extended ensemble method[37] and a thermodynamic integration.[38] The related sampling of the path $(\mathbf{x}_0\cdots\mathbf{x}_t)$ variables needed for this purpose [see Eq. (12)] is performed using a normal-mode sampling.[39,40]

C. The comparison of calculated rate coefficients

Figure 3 compares the values of the thermal rate coefficient $k(T)$, calculated using the various methods, among

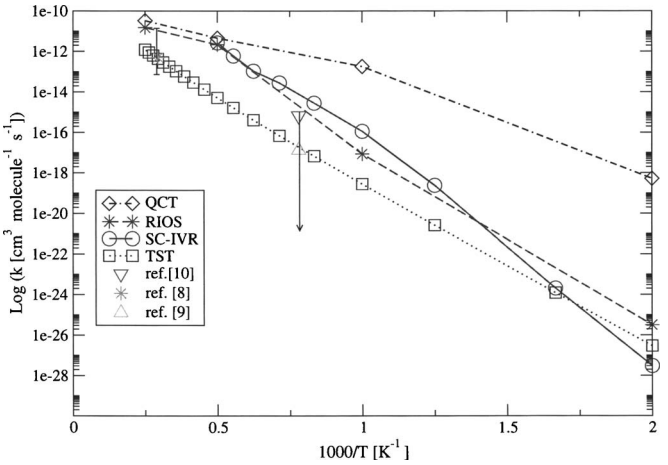

FIG. 3. TST (squares connected by dotted lines), SC-IVR (circles connected by solid lines), RIOS (stars connected by dashed lines), and QCT (diamonds connected by double dashed dotted lines) thermal rate coefficient estimates for the $N+N_2$ reaction plotted as a function of the inverse temperature. The cross and the up and down empty triangles represent the experimental data (related error bars are taken from Ref. 12).

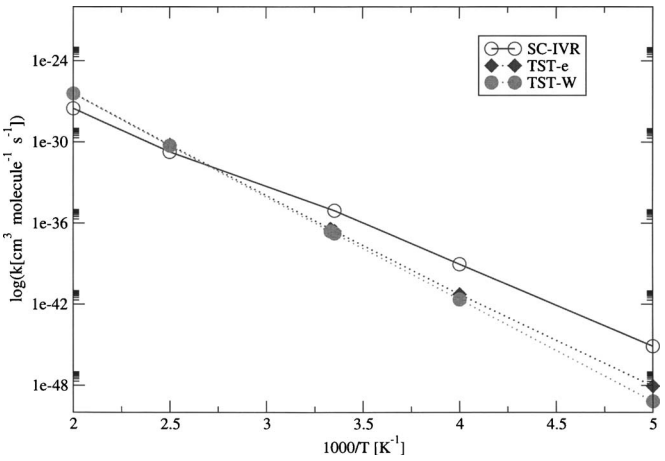

FIG. 4. TST with Wigner and Eckart corrections (solid circles and diamonds, respectively, connected by dotted lines) and SC-IVR (empty circles connected by solid lines) rate coefficients for the $N+N_2$ reaction plotted as a function of inverse temperature.

them and to the experimental data of Lyon[9] (triangle down), Back and Mui[10] (triangle up), and Nan and Lifshitz (cross).[8]

The figure clearly shows the difference (of several orders of magnitude) between calculated and measured values of the rate coefficient. This makes it impossible to draw clear conclusions about the validity of the PES used or the accuracy of the measurements. The only meaningful comparison is therefore that among the various theoretical values. Figure 3 clearly shows that from low to moderate high temperatures QCT calculations overestimate, of some orders of magnitude, the value of the rate coefficient obtained from TST and RIOS quantum ones.

It also shows that, instead, the agreement between TST and RIOS results is definitely better (with the exception of the high temperature region) than expected on the basis of the simplifications made in the TST treatment. However, the most interesting result is the fact that, in spite of being based on trajectory calculations, the SC-IVR method can valorize those classical mechanics outcomes which better relate to quantum effects.

Figure 4 further extends the comparison of our SC-IVR calculations (empty circles connected by a solid line) to lower temperatures by considering the two different (Wigner and Eckart) tunneling corrected TST results. The curves show the satisfactory agreement of TST and SC-IVR values in the very low temperature region (the difference between the two tunneling corrected TST values is very little for the $N+N_2$ reaction).

IV. CONCLUSIONS

In this paper we discuss the possible approaches to the calculation of rate coefficients of elementary reactions based on the structuring of the computation in a way that allows to distribute on the grid various calculations. To this end, we have compared the outcome of SC-IVR calculations with RIOS reduced dimensionality quantum, TST (including tunneling corrections), and full dimensional QCT ones. From the comparison it can be concluded that the SC-IVR method effectively extracts from classical results the features important to mimic quantum effects. This has motivated us to extend the calculations (related work is in progress) to asymmetric and larger systems by considering both isotopic variants (mass asymmetry) and atoms of different nature (electronic asymmetry).

ACKNOWLEDGMENTS

This work has been supported by the MIUR CNR strategic Project L 499/97-200 on High Performance Distributed Enabling Platforms. Thanks are also due to COST in Chemistry, ASI, and the Centre de Computació di Catalunya CESCA for computational resources. One of the authors (N.F.L.) acknowledges the financial support provided through a postdoctoral fellowship from the Basque Government.

[1] A. Laganà, L. Pacifici, and D. Skouteris, Lect. Notes Comput. Sci. **3044**, 357 (2004).
[2] D. Giordano and L. Maraffa, Proceedings of the AGARD-CP-514 Symposium in Theoretical and Experimental Method in Hypersonic Flows 1992, Vol. 26, p. 1.
[3] I. Armenise, M. Capitelli, E. Garcia, C. Gorse, A. Laganà, and S. Longo, Chem. Phys. Lett. **200**, 597 (1992).
[4] M. Capitelli, *Theory of Chemical Reaction Dynamics*, 1st ed. (Springer-Verlag, Berlin, 1996), Vol. 1.
[5] F. Esposito and M. Capitelli, Chem. Phys. Lett. **302**, 49 (1999).
[6] N. Balucani, M. Alagia, L. Cartechini, P. Casavecchia, G. G. Volpi, K. Sato, T. Takayanagi, and Y. Kurosaki, J. Am. Chem. Soc. **122**, 4443 (2000).
[7] N. Balucani, M. Alagia, L. Cartechini, P. Casavecchia, and G. G. Volpi, J. Phys. Chem. A **104**, 5655 (2000).
[8] E. B. Nan and A. Lifshitz, J. Chem. Phys. **47**, 2878 (1969).
[9] R. K. Lyon, Can. J. Chem. **50**, 1437 (1972).
[10] R. A. Back and J. Y. P. Mui, J. Phys. Chem. **66**, 1632 (1962).
[11] A. Laganà and E. Garcia, ChemPhysChem **98**, 502 (1994).
[12] D. Wang, J. R. Stallcop, W. M. Huo, C. E. Dateo, D. W. Schwenke, and H. Partridge, J. Chem. Phys. **118**, 2186 (2003).
[13] A. Laganà, G. O. de Aspuru, and E. Garcia, AIAA/ASME Joint Thermophysics and Heat Transfer Conference, June 20–23, 1994, Colorado Springs, Colorado (unpublished).
[14] A. Laganá, *Nonequilibrium Processes in Partially Ionized Gases*, edited by M. Capitelli and J. N. Bardsley (Plenum, New York, 1990).
[15] R. T Pack, J. Chem. Phys. **60**, 633 (1974).
[16] A. Laganà, E. Garcia, and O. Gervasi, J. Chem. Phys. **89**, 7238 (1988).
[17] W. H. Miller, J. Chem. Phys. **53**, 3578 (1970).
[18] E. J. Heller, J. Chem. Phys. **94**, 2723 (1991).
[19] E. J. Heller, J. Chem. Phys. **95**, 9431 (1991).
[20] T. Yamamoto and W. H. Miller, J. Chem. Phys. **118**, 2135 (2003).
[21] W. H. Miller, J. Chem. Phys. **61**, 1823 (1974).
[22] T. Yamamoto, J. Chem. Phys. **33**, 281 (1960).
[23] A. Laganà, N. Faginas, and A. Riganelli, Int. J. Quantum Chem. **96**, 547 (2004).
[24] D. G. Truhlar, A. D. Isaacson, and B. C. Garrett, *Theory of Chemical Reaction Dynamics* (CRC, Boca Raton, FL, 1985), Vol. 4, Chap. 2, pp. 65–137.
[25] M. J. Pilling and P. W. Seakins, *Reaction Kinetics* 2nd ed. (Oxford Science, Oxford, 1995).
[26] E. Henon and F. Bohr, J. Mol. Struct.: THEOCHEM **531**, 283 (2000).
[27] C. Eckart, Phys. Rev. **35**, 1303 (1930).
[28] L. Pardo, J. R. Banfelder, and R. Osman, J. Am. Chem. Soc. **114**, 2382 (1992).
[29] H. S. Johnston and J. Heicklen, J. Phys. Chem. **66**, 532 (1962).
[30] P. Barreto, A. Vilela, and R. Gargano, J. Mol. Struct.: THEOCHEM **639**, 167 (2003).
[31] P. R. P. Barreto, A. F. A. Vilela, and R. Gargano, Int. J. Quantum Chem. **103**, 685 (2005).
[32] S. S. Ramalho, A. F. A. Vilela, P. R. P. Barreto, and R. Gargano, Chem. Phys. Lett. **413**, 151 (2005).
[33] S. Sato, J. Chem. Phys. **23**, 592 (1955).
[34] S. Sato, J. Chem. Phys. **23**, 2465 (1955).

[35] P. J. Kuntz, E. M. Nemeth, J. C. Polanyi, S. D. Rosner, and C. E. Young, J. Chem. Phys. **44**, 1168 (1966).
[36] G. G. E. D. O. Harris and W. D. Gwinn, J. Chem. Phys. **43**, 1515 (1965).
[37] A. A. M. A. P. Lyubartsev and S. V. Shevkunov, J. Chem. Phys. **96**, 1776 (1992).
[38] D. Frenkel and B. Smit, *Understanding Molecular Simulation* (Academic, San Diego, 1996).
[39] T. Yamamoto, H. Wang, and W. H. Miller, J. Chem. Phys. **116**, 7335 (2002).
[40] D. M. Ceperley, Rev. Mod. Phys. **67**, 279 (1995).